China Ocean Engineering, Vol.15, No.2, pp.253– 268
 ISSN 0890– 5487.

A Numerical Wave Tank for Nonlinear Waves with Passive Absorption

Chung-Ren CHOU (周宗仁)[a], Ruey-Syan SHIH (石瑞祥)[b]
and John Z. YIM (尹彰)[a] *

[a] *Department of Harbour and River Engineering, National Taiwan Ocean University, Keelung 20224, Taiwan, China*
[b] *Department of Civil Engineering, Tung-Nan Institute of Technology, Taiwan, China*

ABSTRACT

A numerical wave tank with passive absorption for irregular waves is considered in this paper. Waves with spectral shapes corresponding to that of the Mitsuyasu-Bretschneider type are used as the initial condition at one end of the flume. An absorbing boundary is imposed at the other end of the wave flume to minimize reflection. By use of a Lagrangian description for the surface elevation, and finite difference for approximation of the time derivative, the problem is then solved by the boundary element method. The effects of the absorbing boundary are investigated by varying the values of the absorption coefficient μ, and studying the time histories of the surface elevations "recorded" on pre-selected locations.

Key words: *numerical wave tank; absorbing beach; irregular waves*

1. Introduction

Correct estimation of all possible environmental forces that might be subjected to is vital for the stability and durability of oceanic and coastal structures. Among all the forces these structures might encounter during their service life, wave forces are probably the most important. Researchers began to study the problem of wave-structure interaction long ago, and this has remained an active research topic till the present day. Generally speaking, studies of wave-structure interaction can be carried out in one of two ways. Physically, a wave tank together with physical models can be used, or field experiments can be conducted. On the other hand, computer algorithms are used to study this problem numerically. However, in a rather strange way, both these techniques rely nowadays heavily on computers.

In earlier years, generation of waves in laboratories can only be achieved through mechanically controlled wave paddles. These paddles can move only monotonously, so that only regular waves can be generated. However, ocean waves are of irregular nature. The irregularities demonstrate themselves through the enhanced crests and flattened troughs, as well as through the irregular water surface. Benefiting from both the advances of controlling techniques in mechanical engineering, and computing speeds in computer technology, devices with different degrees of sophistication have been developed. These devices are capable of generating wave fields that are more realistic in the laboratory. A review concerning the evolution of wave generation techniques in two-dimensional flumes can be found in Mansard and Funke (1988).

In a similar way, although started some forty years ago, numerical simulation of water wave problems has enjoyed its boom for the past two decades also from the advance of the

* Corresponding author, e-mail: b0052@mail.ntou.edu.tw

computer technology. Madsen (1970) studied numerically the problem of water wave generation and subsequent propagation. Periodic waves were generated by a piston-type wavemaker. He used linearized governing equations in his analysis. The result is, therefore, highly idealized, Johnson (1972) numerically solved a variable coefficient Korteweg-de Vries equation, showing that the result can be used to describe the moving of a solitary wave onto a shelf. The problem of sloshing in a water tank was considered by Faltinsen (1978) using the boundary integral equation. Nakayama (1983) used the boundary element method to study the nonlinear water wave problem. In his study, a velocity potential was assumed but the initial boundary condition was kept nonlinear. Based on the boundary integral equation, Brorsen and Larsen (1987) presented a new approach to solve the problem of generation of nonlinear regular waves. Okamura and Yakuwa (1987, see also Sugino and Tosaka, 1990) analyzed the problem of generation, propagation, and subsequent deformation of solitary waves in a water tank using the boundary element method. Invoking Green's theorem, Isaacson *et al.* (1993) used a time-domain second-order method to simulate the propagation of nonlinear waves in a flume. Chou and Shih (1996) analyzed the generation and deformation of solitary waves by means of the boundary element method. Their analysis was based on the Lagrangian description with time derivative. Recent and fairly comprehensive reviews on numerical wave tank studies can be found in Grilli and Horrillo (1997) and Kim *et al.* (1999).

One of the major difficulties encountered in wave generations, either numerical or mechanical, is that they both have boundaries. Wave reflections and re-reflections from the boundaries can obscure and interact with waves generated from the paddle and make the results thus obtained unusable. Researchers noticed this problem long time ago, and uncountable efforts have been made to minimize reflection. A survey of the wave energy absorbing devices commonly used in laboratories can be seen in Ouellet and Datta (1986). The same idea has also been adopted by researchers in numerical wave tanks. Clément (1999), in his review of the numerical wave absorption techniques commonly used by researchers, has divided them into four categories. These are: the numerical beach or sponge layers, active piston absorber, mesh stretching, and other methods. In the present analysis, the idea of numerical beach, or a sponge layer is adopted. This is accomplished through imposing some extra terms in the kinematic and dynamic boundary conditions.

Le Méhauté (1972) seems to be the first one who brought up the idea of an absorbing beach. Later, Larsen and Dancy (1983; see also Brorsen and Larsen, 1987) adopted this idea in their simulation of the generation of nonlinear gravity waves. Based upon the Boussinesq equation, Karambas and Koutitas (1992) modelled the propagation of breaking waves. They used an empirical equation for the dissipation of excessive wave energy. It was shown that good agreement between numerical and experimental results could be achieved. The applicability of their model is, however, limited only for breaking waves on a sloping beach. Grilli and Horrillo (1997), in their simulation of the generation and absorption of fully nonlinear periodic waves, used a dissipative device at the end of their flume. This dissipative device is a combination of an absorbing beach and a piston-like boundary condition. Kim *et al.* (1999) pointed out that, absorbing beaches are more efficient in damping high-frequency waves, whereas radiation type boundaries are good for low-frequency waves. A combination of these two devices should, therefore, be more effective in damping both high and low frequency waves. The results of Grilli and Horrillo (1997) seem to confirm this.

In this paper, the idea of a sponge layer is adopted in the analysis of numerical generation of irregular waves. The absorbing coefficient μ is further divided into two sections —a changing section, where μ changes gradually, and a constant value section, where it remain constant. In the following, we further divide the rest of the paper into three sections. In section 2, the numerical scheme is described briefly; the results are presented in Section 3, together with discussions. And in Section 4 some conclusions are drawn from the present analyses.

2. Numerical Analyses

2.1 Governing Equations

As can be seen from Fig. 1, a pseudo-wavemaker is located at the right-hand end of the flume. The positive x-axis is pointed to the right, whereas the z-axis is pointed positively upwards, with the origin of the coordinate system located on the still water level (SWL). A vertical wall is located at the left end of the flume, opposite to the wavemaker. The bottom floor is assumed to be impermeable. The regime of interest is therefore bounded by the wavemaker at the right Γ_1, the free water surface Γ_2 atop, the vertical wall at the left Γ_3, and the impermeable bottom floor Γ_4.

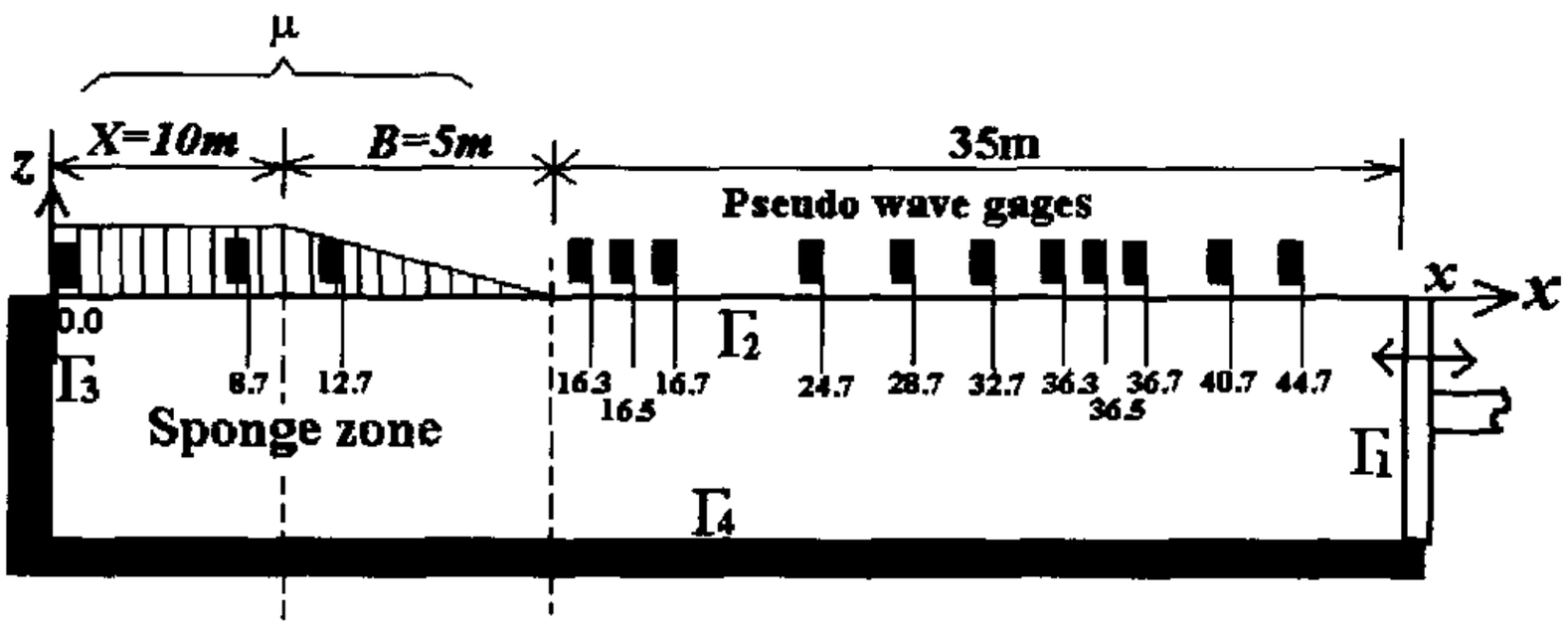

Fig. 1. Schematic representation of the numerical tank.

The fluid is assumed to be inviscid, and the motion irrotational as has been usually done. Accordingly, a velocity potential $\Phi(x, z, t)$ exists, which satisfies the Laplace equation:

$$\frac{\partial^2 \Phi}{\partial x^2} + \frac{\partial^2 \Phi}{\partial z^2} = 0 . \tag{1}$$

The kinematic and dynamic free-surface boundary conditions can be expressed in the Lagrangian form:

$$u = \frac{\mathrm{D}x}{\mathrm{D}t} = \frac{\partial \Phi}{\partial x} , \tag{2}$$

$$w = \frac{\mathrm{D}z}{\mathrm{D}t} = \frac{\partial \Phi}{\partial z} \,, \tag{3}$$

$$\frac{\mathrm{D}\Phi}{\mathrm{D}t} + g\zeta - \frac{1}{2}\left[\left(\frac{\partial \Phi}{\partial x}\right)^2 + \left(\frac{\partial \Phi}{\partial z}\right)^2\right] + \frac{P}{\rho} = 0 \,. \tag{4}$$

In the above expressions, D(•) is the Lagrangian derivative; u and w are, respectively, the horizontal and vertical velocity components of the water particle, g is the gravitational acceleration, with η representing the surface fluctuation, ρ the density, and P the pressure on the fluid surface.

2.2 Boundary Conditions

On the vertical and bottom boundaries, which are impermeable, the particle velocity of the fluid normal to it must be zero, thus:

$$\frac{\partial \Phi}{\partial n} = 0 \quad \text{on } \Gamma_3 \text{ and } \Gamma_4 \,. \tag{5}$$

On the surface of the wave paddle, continuity requires that fluid particles follow the velocity of the wave paddle:

$$\overline{\Phi} = \frac{\partial \Phi}{\partial n} = -U(t) \text{ on } \Gamma_1 \,. \tag{6}$$

2.3 The Sponge Zone

The sponge zone is composed of two sections, a gradually varying section, where the value of the absorption coefficient, μ, varies gradually, and a constant-valued absorption coefficient zone. See Fig. 1 for the definition sketch.

Following Cao *et al.* (1993), an external pressure is specified on the dynamic free surface, Eq. (4). This countering acting pressure is defined to be proportional to the normal particle velocity. By doing so, positive work on the fluid body, when this pressure term is assumed to be proportional to the free-surface velocity potential, can be avoided.

$$P(x, \zeta) = \mu(x) \frac{\partial \Phi}{\partial n}\left[\zeta(x)\right] \tag{7}$$

where $\mu(x)$ is the beach absorption function, which is assumed to vary smoothly along the section $x_X - x_B$. Grilli and Horrillo (1997), in their analysis, have used an absorbing coefficient that is a function of both time and space, which, with the present expression, can be written as:

$$\mu(x, t) = \mu_0(t)\, \rho \sqrt{g h_B} \left(\frac{x_B - x}{B}\right)^{\gamma} \tag{8}$$

where $B = x_X - x_B$ is the length of the varying-value section and $\gamma \geqslant 1$. As can be seen from Fig. 1, a value of $\gamma = 1$ is used in the present analysis. The absorbing coefficient is therefore as-

sumed to vary linearly.

2.4 The Numerical Scheme

The continuity equation in the differential form, Eq. (1), can be transformed into a boundary integral equation by the use of Green's second identity. The velocity potential at any point within the domain of computation, $\Phi(x, z, t)$, can be expressed by use of the velocity potential on the boundary, $\Phi(\xi, \eta; t)$, and its normal derivative, $\partial \Phi(\xi, z; t)/\partial n$ through:

$$\Phi(x, z; t)=\frac{1}{2\pi}\int_{\Gamma}\left\{\frac{\partial\Phi(\xi, \eta;\ t)}{\partial n}\ln\left(\frac{1}{r}\right)-\Phi(\xi, \eta;\ t)\frac{\partial}{\partial n}\left[\ln\left(\frac{1}{r}\right)\right]\right\}\mathrm{d}s \tag{9}$$

where $r=\sqrt{(\xi-x)^2+(\eta-z)^2}$. Close to a boundary point (ξ', η'), the velocity potential of this point is expressed through:

$$\Phi(\xi', \eta'; t)=\frac{1}{\pi}\int_{\Gamma}\left\{\frac{\partial\Phi(\xi, \eta;\ t)}{\partial n}\ln\left(\frac{1}{R}\right)-\Phi(\xi, \eta;\ t)\frac{\partial}{\partial n}\left[\ln\left(\frac{1}{R}\right)\right]\right\}\mathrm{d}s \tag{10}$$

where $R=\sqrt{(\xi-\xi')^2+(\eta-\eta')^2}$.

The boundaries, Γ_1 through Γ_4, are divided into, respectively, N_1 to N_4 discrete linear elements. With the introduction of a local dimensionless coordinate, the integral equation can be expressed in the matrix form:

$$[\Phi_i]=[\mathbf{O}_{ij}]\ [\overline{\Phi}_i]\ ; \qquad i, j=1\sim 4 \tag{11}$$

where $[\Phi]$ and $[\Phi]$ are, respectively, the velocity potential and its associated normal derivative. The coefficients of the matrix $[\mathbf{O}]$ are related to the geometric shapes of the boundaries. Detailed expressions of these matrixes can be found in Chou and Shih (1996).

Substituting the initial boundary conditions into Eq. (11) gives the value of the velocity potential on the boundary of the wavemaker, Φ_1^k, the normal derivative of the velocity potential of the free surface, $\overline{\Phi}_2^k$, and the velocity potentials on the fixed impermeable boundaries, Φ_3^k and Φ_4^k at the k-th time step. Differentiating the time derivatives in Eqs. (2), (3) and (4), using forward difference, one obtains the new positions of the free water surface, (x^{k+1}, z^{k+1}), and the velocity potential on the free water surface, Φ_2^{k+1}, at the next time step, $t=(k+1)\Delta t$ as:

$$\Phi_2^{k+1}=\Phi_2^k+\frac{1}{2}\left[\left(\frac{\partial\Phi_2}{\partial s}\right)^2+\left(\frac{\partial\Phi_2}{\partial n}\right)^2\right]\Delta t-gz^{k+1}\Delta t-\frac{P^k}{\rho}\Delta t \tag{12}$$

where s and n denote, respectively, the tangential and the normal direction. The normal derivatives on the boundaries Γ_1, Γ_3 and Γ_4, i. e., $\overline{\Phi}_1^{k+1}$, $\overline{\Phi}_3^{k+1}$ and $\overline{\Phi}_4^{k+1}$, at time step $t=(k+1)\Delta t$ can be obtained by use of Eqs. (5) and (6). These can be written more compactly in a matrix form:

$$\begin{bmatrix} \Phi_1 \\ \bar{\Phi}_2 \\ \Phi_3 \\ \Phi_4 \end{bmatrix}^{k+1} = \begin{bmatrix} \mathrm{I} & -O_{12} & 0 & 0 \\ 0 & -O_{22} & 0 & 0 \\ 0 & -O_{32} & \mathrm{I} & 0 \\ 0 & -O_{42} & 0 & \mathrm{I} \end{bmatrix}^{-1} \begin{bmatrix} O_{11} & 0 & O_{13} & O_{14} \\ O_{21} & -\mathrm{I} & O_{23} & O_{24} \\ O_{31} & 0 & O_{33} & O_{34} \\ O_{41} & 0 & O_{43} & O_{44} \end{bmatrix} \begin{bmatrix} \bar{\Phi}_1 \\ \Phi_2 \\ \bar{\Phi}_3 \\ \bar{\Phi}_4 \end{bmatrix}^{k+1} \tag{13}$$

where I is the identity matrix. the details of the numerical procedures can be found in Chou and Shih (1996).

The computational domain is discretized into, respectively, 11 nodes for both the vertical wall at the left end and the wavemaker on the right hand, 51 nodes for the impermeable bottom, and 239 nodes for the free surface. This is shown schematically in Fig. 2. A constant time step of $\Delta t = 0.0025$ s is used in the computation. It is well known that numerical errors are the function of the size of both the spatial and temporal steps. Researchers have found that these errors can be minimized if the Courant number is kept small. The Courant number can be defined as:

$$\mathrm{Co} = \sqrt{gh}\,\frac{\Delta t}{\Delta x} \leqslant 0.5 \tag{14}$$

where Δx and Δt are the spatial and the temporal discretization interval. According to the present discretization scheme, the Courant number is in the range of $0.157 \sim 0.391$, for $\Delta x = 0.2 \sim 0.5$ m on the free surface. It can therefore be claimed that the stability of the present numerical scheme is guaranteed.

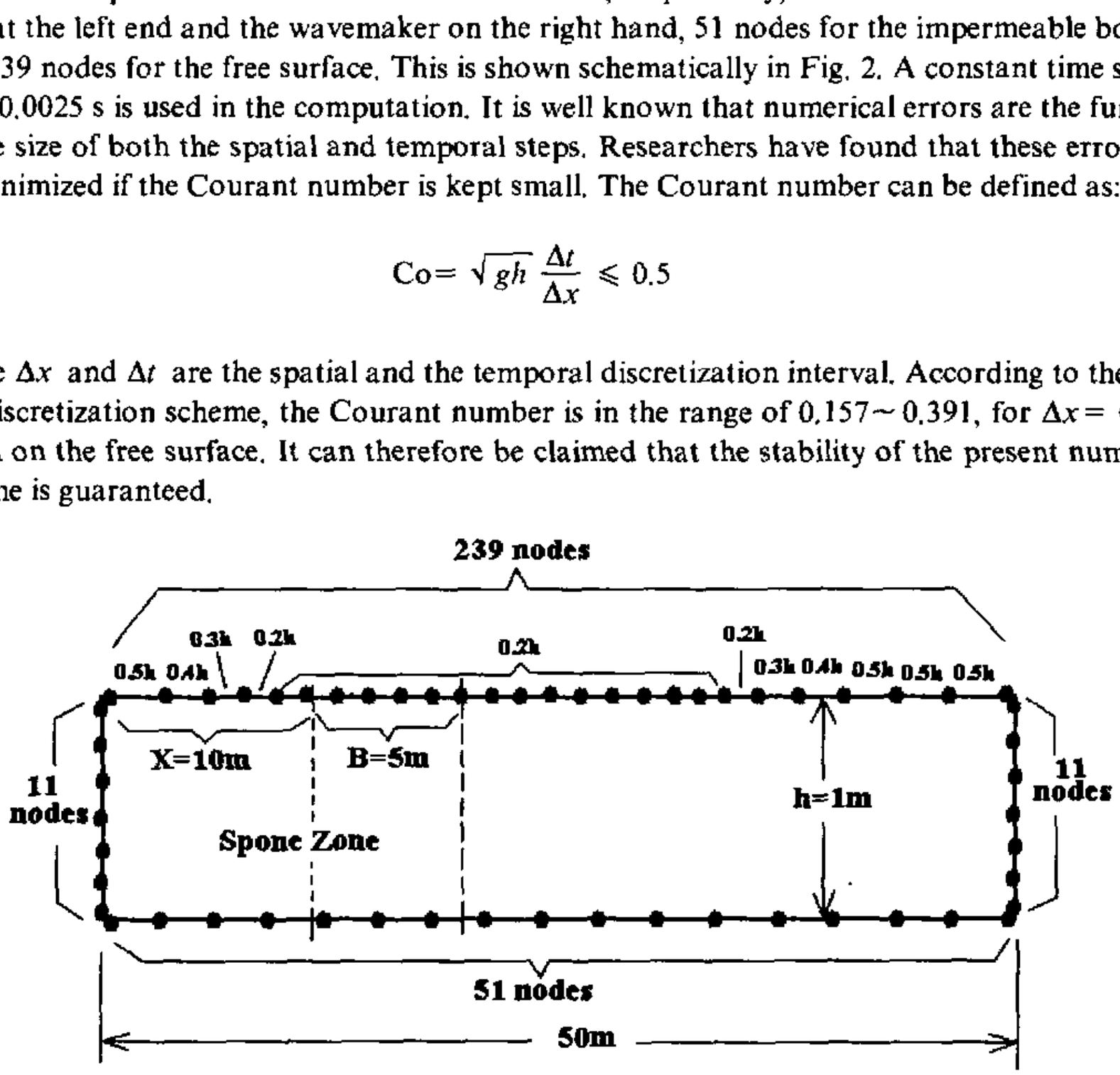

Fig. 2. Scheme for the discretization of the computational domain.

2.5 Random Wave Simulation

The Bretschneider-Mitsuyasu spectrum is used as the target spectrum for the generation of random waves. It can be expressed as

$$S(f) = 0.257 \frac{H_{1/3}^2}{T_{1/3}^4 f^5} \exp\left[-\frac{1.03}{(T_{1/3} f)^4}\right] \tag{15}$$

where $H_{1/3}$ is the significant wave height, $T_{1/3}$ is the associated significant wave period, and f is the frequency. The spectral peak frequency, f_p, is related to the significant wave period through (Goda, 2000)

$$f_p = \frac{1}{1.05 T_{1/3}} \tag{16}$$

In general, the surface fluctuations can be expressed either by use of:

$$\zeta(m\Delta t) = \sum_{j=1}^{N/2} \left[a_j \cos(2\pi j \Delta f m \Delta t) + b_j \sin(2\pi j \Delta f m \Delta t) \right] \tag{17}$$

or through

$$\zeta(m\Delta t) = \sum_{j=1}^{N/2} \left[A_j \cos(2\pi j \Delta f m \Delta t + \varphi_j) \quad j = 1, \ldots, N \right. \tag{18}$$

where

$$\Delta f = \frac{1}{N\Delta t} \tag{19}$$

in the frequency resolution, Δt is the time discretization, $T = N\Delta t$ is the total length (time) of the surface records, N is the total number of sampling points in the time domain, and $m = 1, 2, \ldots, N$. In Eq. (17), both the amplitudes, a_j and b_j are independent random variables that are normally distributed with zero mean, with standard deviation equal to

$$\sigma_j = \sqrt{S(2\pi j \Delta f)\, 2\pi \Delta f}\,. \tag{20}$$

The amplitude A_j in Eq. (18) is directly related to the spectral density through

$$A_j = \sqrt{2S(2\pi j \Delta f)\, \Delta\omega} = 2\sqrt{S(2\pi j \Delta f)\, \pi \Delta f} \tag{21}$$

and the phases φ_j are assumed to have a uniform distribution with zero mean and unit variance, i. e., $\varphi_j \sim 2\pi U[0,1]$. Depending on whether Eqs. (17) or (18) is used, the random wave simulation procedure is either non-deterministic or deterministic (Tuah and Hudspeth, 1982). In this study the latter method is adopted.

Similar to that in physical applications of the wave generation theory, a transfer function must be multiplied to obtain the spectrum for the motion of the wave generator

$$S'(f) = \alpha(f) S(f) \tag{22}$$

where $\alpha(f)$ denotes the transfer function. From linear, i. e., first-order, theory, $\alpha(f)$ is equal to (Hughes, 1993)

$$\alpha(f) = \left[m_1(f) \right]^2 \tag{23}$$

where $m_1(f)$ is the transfer function of the wave amplitude and the stroke of wave-generator St. For a piston type wave generator

$$m_1 = \frac{a_j}{St_j} = \frac{2\sinh^2(kh)}{\sinh(2kh) + 2kh} \tag{24}$$

where a_j is the respective amplitude of the associated frequency components and h is the water depth. The frequency dependence of the transfer function is omitted for simplicity. The wavenumber k is related to the frequency f through the linear dispersion relation

$$\omega^2 = gk \tanh(kh) \tag{25}$$

In this study, four significant wave periods have been used in combination with six values of the absorbing coefficients. Table 1 summarizes the experimental conditions used in the numerical experiments. As can be seen from Table 1, a total of 24 numerical experiments have been carried out.

Table 1 Conditions used for the numerical experiments

Significant wave height $H_{1/3}$ (cm)	Significant wave period $T_{1/3}$ (sec)	Absorbing coefficient (μ)					
10	1.2	0.0	0.025	0.05	0.10	0.15	0.20
10	1.3	0.0	0.025	0.05	0.10	0.15	0.20
10	1.4	0.0	0.025	0.05	0.10	0.15	0.20
10	1.5	0.0	0.025	0.05	0.10	0.15	0.20

3. The Numerical Analysis

3.1 Analysis of Results

A 50-meter long numerical wave tank is used in this study. The water depth is 1.0 meter. Facing the wave tank, a piston wave generator is located at the right hand end, while a vertical impermeable wall is at the left end. To dissipate wave energy incident from the right-hand end, an absorbing beach is imposed on the left-hand end. As mentioned earlier, this absorbing beach, composed of imaginary external pressure, is divided into a gradually varying section and a constant value section. The former has a length of 5 meters, and the latter is 10 m long.

To monitor the development of irregular waves along the wave tank, a total of 14 wave stations are selected. They will be called, starting from the still position of the piston, Stations 1～14 hereafter. Table 2 lists the number of the stations and their respective distances away from the vertical wall at the left end of the wave flume. Stations 9～11 are used to determine possible reflections from the absorbing beach; whereas Stations 3～5 are used for the same purpose but are, however, for reflections from the wavemaker.

Table 2 The pseudo wave stations and their locations

Station No.	14	13	12	11	10	9	8	7	6	5	4	3	2	1
Distance (m)	0	8.7	12.7	16.3	16.5	16.7	24.7	28.7	32.7	36.3	36.5	36.7	40.7	44.7

Recordings of surface fluctuations start as soon as wave generation has been initiated, and this is done simultaneously for all wave gauges. After surface fluctuations are obtained from calculation, spectral analyses are performed. In an attempt to increase the degrees of freedom (DOF) in the spectral estimates, wave records are first divided into segments with 50% over-lapping (Otnes and Enochson, 1972). Then, a partial cosine taper function is added to each segment so that side-lobe leakage can be minimized (Bendat and Piersol, 1986). The data are Fast Fourier Transformed (FFT), and a rough, two-sided spectral estimate can be obtained. A smooth estimate of the spectral density can then be obtained through ensemble averaging. A final smoothing of the spectral densities is carried out in the frequency domain using a Hanning window (Bendat and Piersol, 1986).

Depending upon the discretization time interval of the wave records, Δt, the DOF of the spectral estimates ranges from 2 to 44, whereas the associated frequency resolution, is, respectively, $\Delta f = 0.0195313 \sim 0.3125$ Hz.

3.2 Results and Discussion

Owing to the large amount of calculated data, we will, therefore, concentrate ourselves on results obtained at Station Nos. 1, 6, 9 and 13. As can be seen from Fig. 1. Station No. 1 is situated just in front of the wavemaker, and Station No. 6 is located approximately in the middle of the section between the wavemaker and the absorbing beach. For illustration of the effect of the absorbing beach, Station No. 9, which is in front of it, and Station No. 13, which is within the constant-coefficient section of the absorbing beach, are chosen.

Figs. 3A~3D show the developments of random waves along the wave tank. Waves under consideration have a significant period of $T_{1/3} = 1.2$ s, with a significant wave height of $H_{1/3} = 10$ cm. The absorbing coefficient for this case is $\mu = 0$. From Fig. 3 it can be seen that, with increasing distance away from the wavemaker, the number of waves decreases. The exact reason for this result is not clear at present. It is conjectured that this is probably due to the fact that simulated random waves contain too many so-called "false waves" (Giménez *et al.*, 1994; Pires-Silva and Medina, 1994). This can be clearly seen from Fig. 3A at $t = 4 \sim 10$, $15 \sim 17$ and $42 \sim 50$ seconds. As pointed out by those authors (see also Medina *et al.*,1995) the existence of these false waves will not only seriously distort the statistical properties of the wave field, but an increasingly broader energy spectrum will also result with the increasing number of false waves contained in the "wave record".

There is another plausible explanation for the decrease of the number of waves with, however, increasing wavelengths for records measured at downstream stations. Since the surface elevations are composed of linear waves, the waves with larger wavelengths will naturally travel faster and reach the downstream end earlier. In our numerical simulations, calculations are often forced to terminate when reflected waves have reached the wavemaker. Since the present wave tank is rather short, 50 m, only a limited number of waves will be present in the flume. As a result, the downstream stations can measure only waves with large wavelengths.

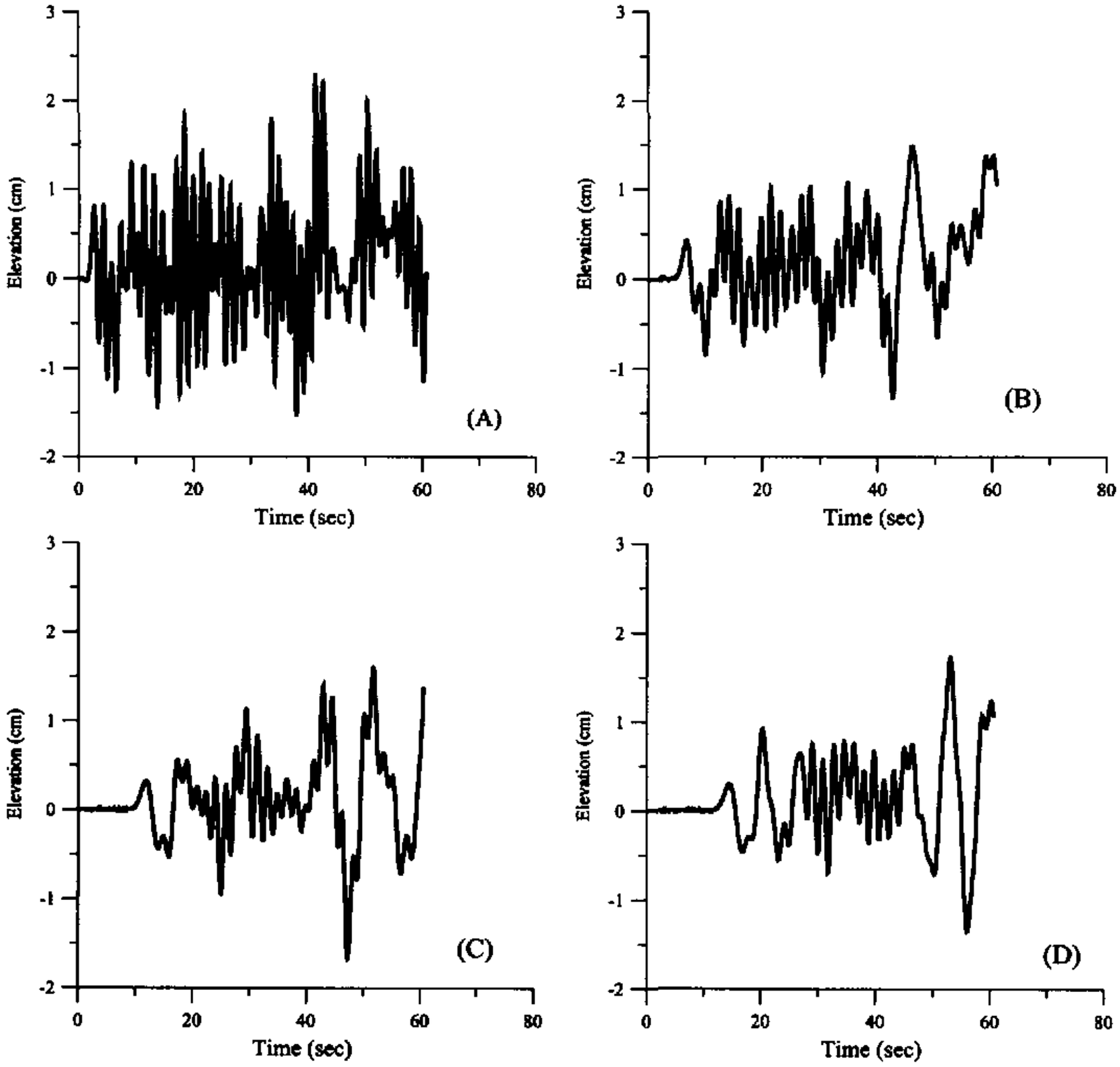

Fig. 3. Evolutions of irregular waves along the wave tank.
Figs. 3A~3D: station Nos. 1, 6, 9 and 13.
Case studied: Bretscheider-Mitsuyasu spectrum with $H_{1/3}$ = 10 cm,
$T_{1/3}$ = 1.2 s, without absorbing beach, i. e., $\mu = 0$.

Figs. 4A~4D are the estimated spectral densities of the wave records shown in Figs. 3A~3D. As can be seen from these figures, the spectral peak moves progressively toward lower frequencies. It is believed that the reason for this to occur is, as stated above, only longer waves with faster phase speeds can be measured by these stations.

For demonstration of the effect of the magnitude of the absorbing coefficient on the development of waves, three different values of μ are chosen. These are shown in Figs. 5~8, for, respectively, $\mu = 0.025$ and 0.20. It can be seen from these figures that, with the implantation of the absorbing beach, the energies of waves decrease. Figs. 5 and 7 show the development of irregular waves along the flume. The waves shown in these figures have significant periods of 1.3 and 1.5 seconds, respectively. It can be seen that there is an upward trend occurring in the wave

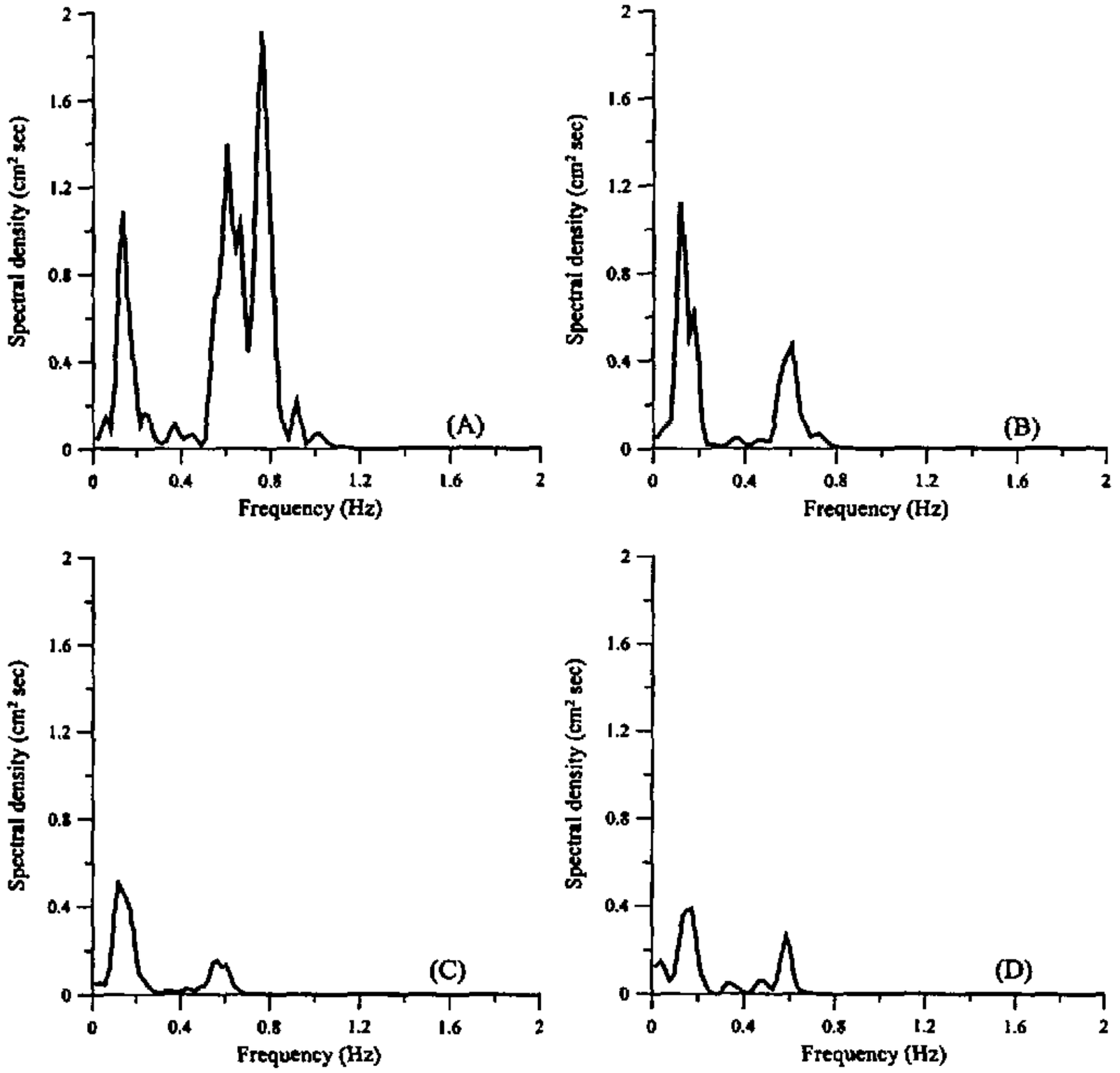

Fig. 4. Spectral densities of irregular waves along the wave tank.
Fig. 4A～4D: station Nos. 1, 6, 9 and 13. Case studied: same as Fig. 3.

flume. This can be clearly seen from the figures of surface fluctuations measured at the far end of the flume, i. e., Station No. 13, as shown in Figs. 5D and 7D. The exact cause of this trend is not clear. As mentioned earlier, the time series are trend-removed prior to spectral analyses. The fact that this trend remains even after this procedure indicates that, an up to 5^{th} order polynomial approximation of the trend is ineffective in its removal. Since, however, this upward trend is absent in the absence of the absorbing beach, it must be caused by its presence. Furthermore, it is found that, as the magnitude of the absorbing coefficient, μ, increases, the slope of this trend also increases (not shown here). Grilli and Horrillo (1997) pointed out that the use of the fully nonlinear boundary conditions will lead to a net mass transport of the calculated results. Whether this is the reason for the existence of the trend must await further investigation.

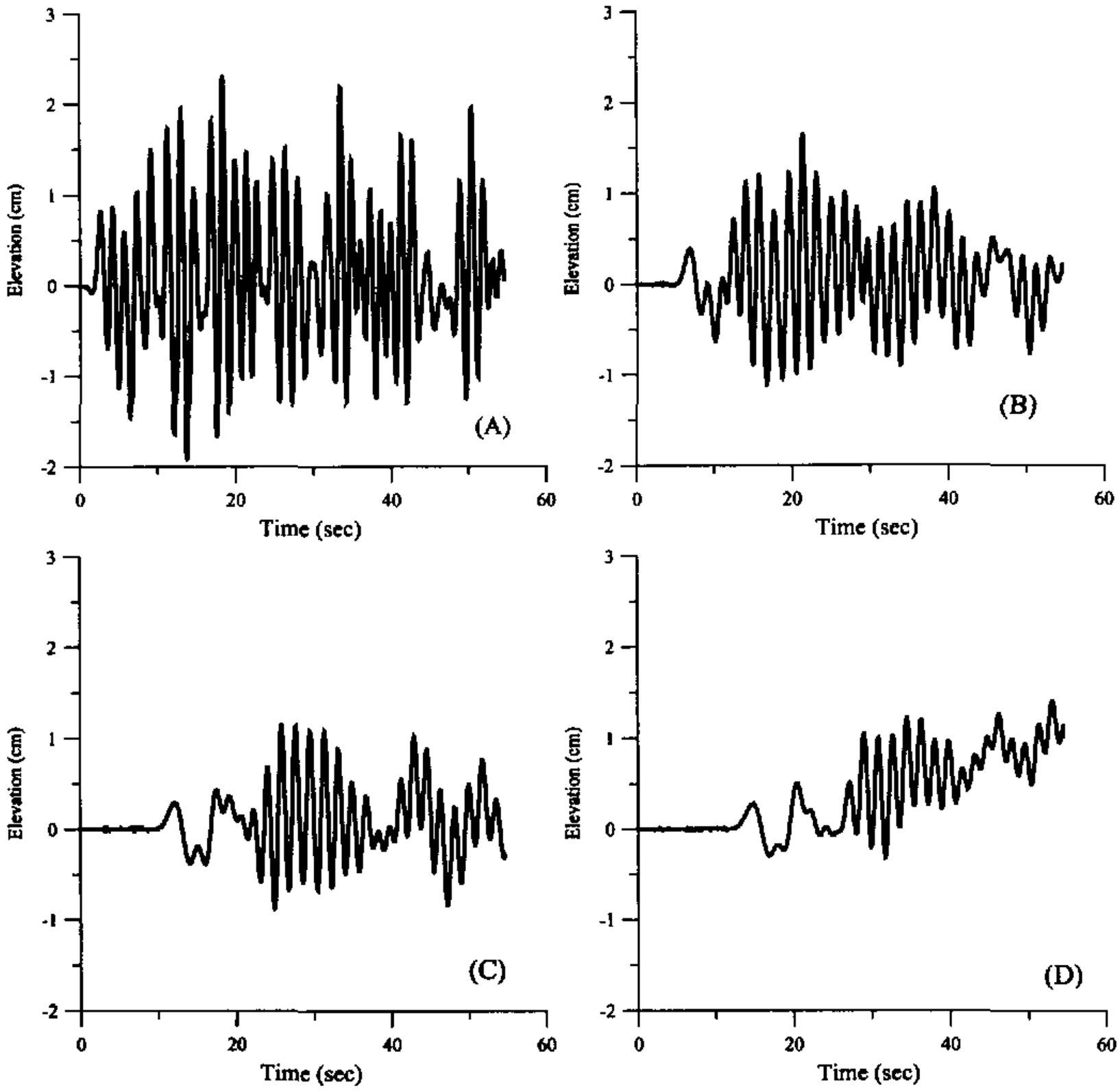

Fig. 5. Evolutions of irregular waves along the wave tank.
Figs. 5A~5D: station Nos. 1, 6, 9 and 13.
Case studied: Bretschneider-Mitsuyasu spectrum with $H_{1/3} = 10$ cm, $T_{1/3} = 1.3$ s, with absorbing beach, i. e., $\mu = 0.025$.

Spectral densities corresponding to the developments of random waves shown in Figs. 5 and 7 are shown in Figs. 6 and 8, respectively. A couple of interesting points are worth mentioning

— Unlike for the case with the lowest significant wave period, $T_{1/3} = 1.2$ sec, the spectral shapes for Station Nos. 1 and 2 have an appearance close to that of wind waves.

— As waves evolve, their spectral densities diminish. The larger the magnitude of the absorbing coefficient, the faster the rate for the energy to decrease.

— The effect of the upward-going trend can also be clearly seen through the increase of the spectral density near low frequencies.

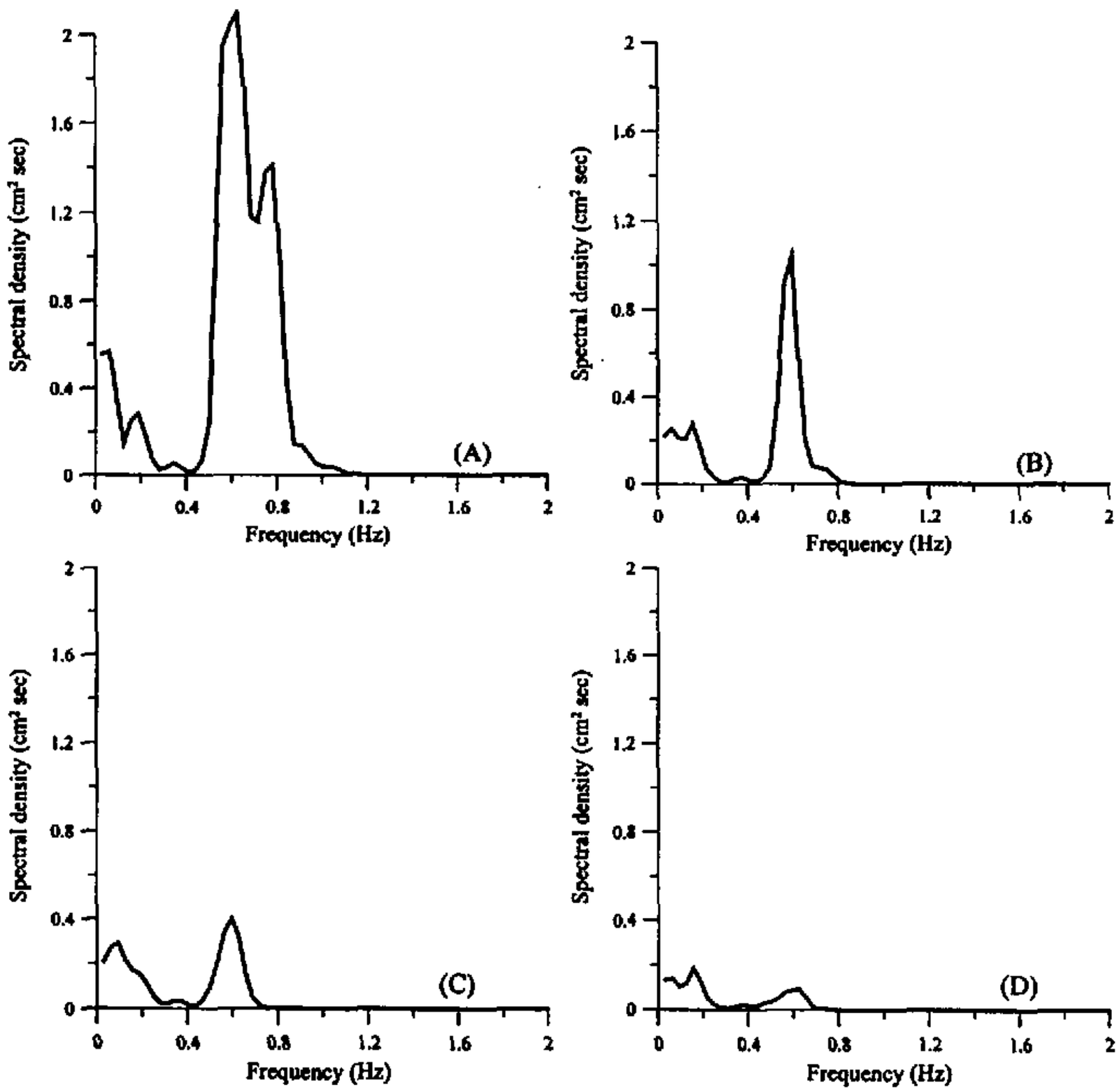

Fig. 6. Spectral densities of irregular waves along the wave tank.
Figs. 6A~6D: station Nos. 1, 6, 9 and 13.
Case studied: same as Fig. 5.

4. Conclusions

Generation and propagation of random waves along a wave tank are studied with the boundary element method. The Bretschneider-Mitsuyasu spectrum is used as the target for simulation of random waves to be generated by a piston. Incident wave energies are dissipated through an absorbing beach at the other end of the wave tank. The efficiency of the absorbing beach is studied by varying the values of the absorbing coefficient. It is concluded that

—The process of random wave generation and dissipation can be studied with the boundary element method. It is demonstrated that with the implantation of a sponge layer at the other end of the flume, the wave energy will be damped, and the duration of simulation thereby elongated. However, it is found that.

—A 50 m numerical wave tank is probably too short for simulation of random wave gener-

ation. For the wave data used in this study, according to Eq. (16) the waves with the lowest significant period, $T_{1/3} = 1.2$ sec have a peak frequency of $f_p \approx 0.8$ Hz. This corresponds to a phase

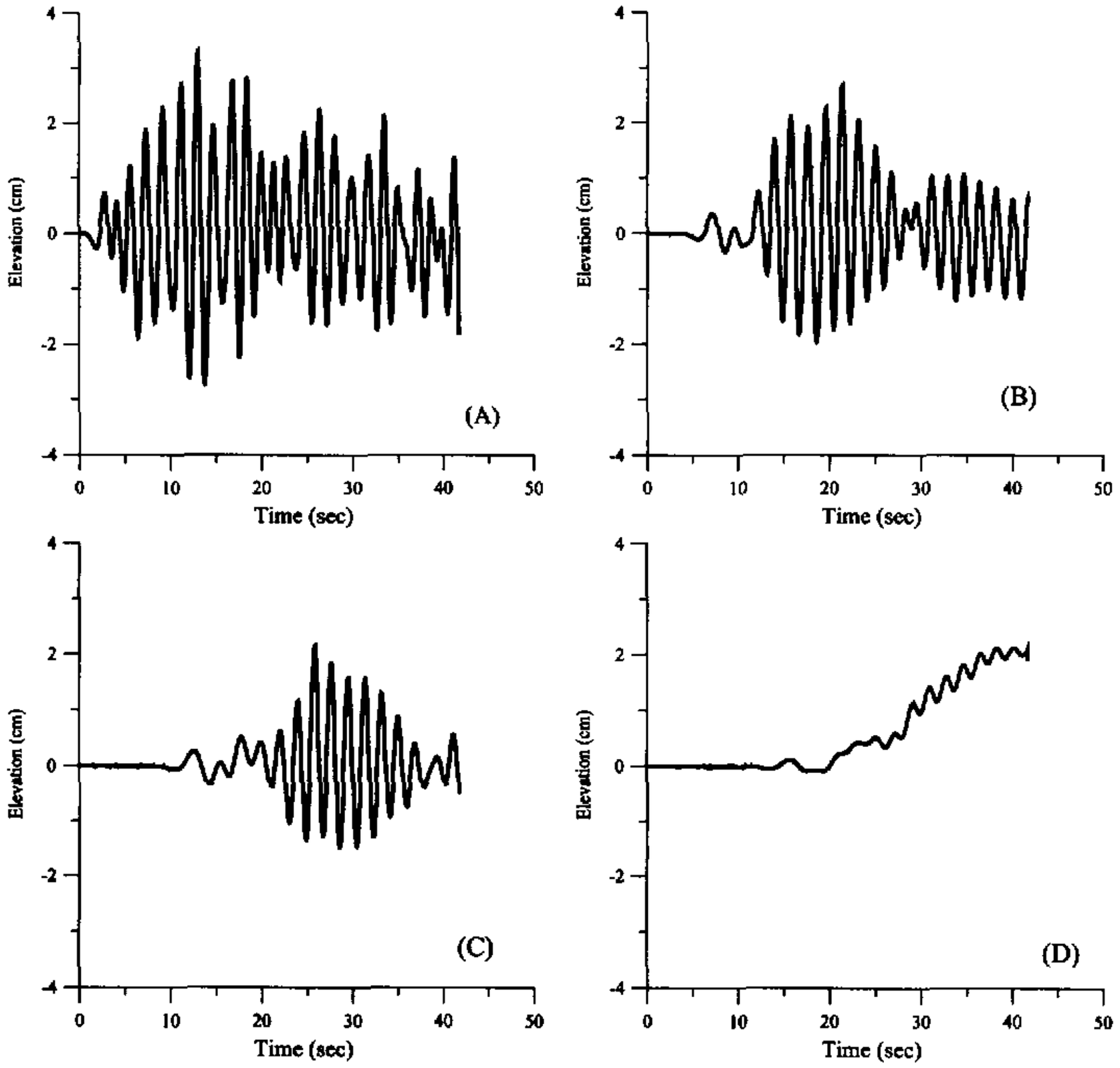

Fig. 7. Evolutions of irregular waves along the wave tank.
Figs. 7A~7D: station Nos. 1, 6, 9 and 13.
Case studied: Bretschneider-Mitsuyasu spectrum with $H_{1/3} = 10$ cm, $T_{1/3} = 1.5$ s, with absorbing beach, i. e., $\mu = 0.20$.

velocity of $C_0 \approx 195.2$ cm / sec in deep water. The waves will therefore reach the end of the wave tank in approximately 25 sec. Since the length of dominant waves is 244 cm, a rough estimate shows that there will be only 40~ 50 dominant waves in the wave tank when reflected waves reach the wavemaker. It is conjectured that with this amount of waves the estimated spectral densities could be biased (Goda, 2000).

— An absorbing beach, or sponge layer, at the far end of the wave flume can effectively decrease wave energy in the flume.

— However, there is an upward trend associated with the implantation of the sponge layer

at the other end of the flume. The slope of this upward trend increases with the increasing value of the absorbing coefficient. The exact reason for this upward trend to occur is not clear at present.

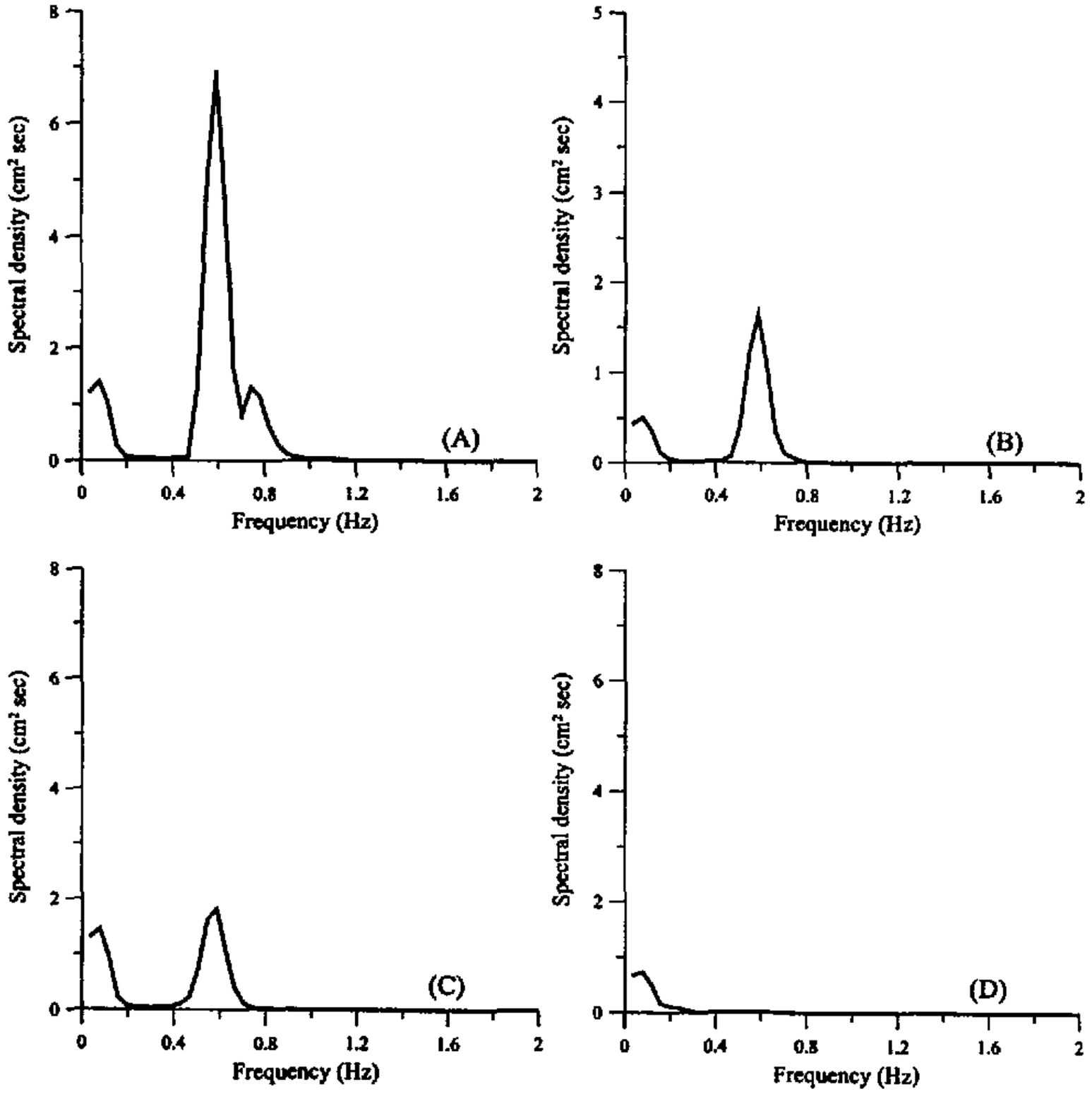

Fig. 8. Spectral densities of irregular waves along the wave tank.
Figs. 8A~8D: station Nos. 1, 6, 9 and 13.
Case studied: same as Fig. 7.

—Concentration of energy in the low frequency part of the spectra seems to indicate that there are long waves in the numerical tank. Kim *et al.* (1999) pointed out that, numerical beaches are ideal for absorbing energies of short waves, and fail to work for long waves. To absorb the energy of long waves, an active wave absorber must be installed at the end of the flume opposite to the wavemaker. This will be studied in the near future.

Acknowledgements —The authors wish to express their gratitude for the financial aid of the National Science Council, China. Project Nos. NSC-89-2611-E-019-027 (CRC) and NSC-89-2611-E-019-058 (JZY).

References

Bendat, J. S. and Piersol, A. G., 1986. *Random Data Analysis and Measurement Procedures*, 2nd ed. John Wiley, New York, 566.

Brorsen, M. and Larsen, J., 1987. Source generation of nonlinear gravity waves with the boundary integral equation method, *Coastal Engineering*, **11** (4): 93~113.

CAO, Y., Beck, R. F. and Schultz, W. W., 1993. An absorbing beach for numerical simulations of nonlinear waves in a wave tank, *Proc. 8th Int. Workshop Water Waves and Floating Bodies*, 17~20.

CHOU, C. R. and Shih, R. S., 1996. Generation and deformation of solitary waves, *China Ocean Engineering*, **10** (4): 419~432.

Clément, A. H., 1999. Benchmark test cases for numerical wave absorption: 1st Workshop of ISOPE numerical wave tank group, Montréal, May 1998 Proc. 9th Int'l Offshore and Polar Engineering Conf., Brest, Vol. Ⅲ, 266~289.

Faltinsen, O., 1978. A numerical nonlinear method of sloshing in tanks with two-dimensional flow, *J. Ship Res.*, **33** (3): 193~202.

Giménez, M. H., Sanchez-Carratala, C. R. and Medina, J. R., 1994. Analysis of false waves in numerical sea simulations, *Ocean Engineering*, **21**, 751~764.

Goda, Y., 2000. *Random seas and design of maritime structures*, 2nd ed., World Scientific, Singapore, 443.

Grilli, S. T. Horrillo, J., 1997. Numerical generation and absorption of fully nonlinear periodic waves, *J. Eng. Mech.*, ASCE, **123**, 1060~1069.

Grilli, S. T. and Subramanya, R., 1995. Recent advances in the BEM modeling of nonlinear water waves, *BE Applications in Fluid Mechanics*, Chapter 4, 91~122.

Hughes, S. A., 1993. *Physical models and laboratory techniques in coastal engineering*, World Scientific Pub. Co., Singapore, 568.

Isaacson, M., Cheung, K. F., Mansard, E. and Miles, M. D., 1993. Transient wave propagation in a laboratory flume, *J. Hydraulic Res.*, **31**, 665~680.

Johnson, R. S., 1972. Some numerical solutions of a variable-coefficient Korteweg-de Vries equation (with applications to solitary wave development of a shelf, *J. Fluid Mech.*, **54**, 81~91.

Karambas, Th. V. and Koutitas, C., 1992. A breaking wave propagation model based on the Boussinesq equation, *Coastal Engineering*, **18**, 1~19.

Kim, C. H., Clément, A. H. and Tanizawa, K., 1999. Recent research and development of numerical wave tanks —a review, *Int J. Offshore and Polar Eng.*, **9**, 241~256.

Larsen, J. and Dancy, H., 1987. Open boundaries in short wave simulations —A new approach, *Coastal Engineering*, **7**, 285~297.

Madsen, O. S., 1970. Wave generation by a piston type wavemaker, *Proc. 12th International Conf. Coastal Engng.* Washington, ASCE, New York, 589~607.

Mansard, E. P. D. and Funke, E. R., 1988. *A rational for the use of the deterministic approach to laboratory wave generation*, in Selected papers on two-dimensional wave generation and analysis, Report NRCC No. 28750, Hydraulic Laboratory, National Research Council Canada, Ottawa, 1~44.

Medina, J. R., Aguilar, J. and Diez, J. J., 1995. Distortions associated with random sea simulations, *J. Waterway, Port, Coastal and Ocean Eng.*, ASCE, **111**, 603~628.

Le Méhauté, B., 1972. Progressive wave absorber, *J. Hyd. Res.*, **10**(2): 153~169.

Nakayama, T., 1983. Boundary element analysis of nonlinear water wave problem, *Int J. for Numerical Method in Engineering*, **19**, 953~970.

Otnes, R. K. and Enochson, L., 1972. *Digital time series analysis*, John Wiley and Sons., New York, 467.

Ouellet, Y. and Datta, I., 1986. A survey of wave absorbers, *J. Hydraulic Res.*, **24**, 265~280.

Pires-Silva, A. A. and Medina, J. R., 1994. False waves in wave records, *Ocean Engineering.*, **21**, 765~770.

Sugino, R. and Tosaka, N., 1990. Boundary element analysis of nonlinear water wave problem, *Pacific Congress on Marine Science and Technology*, PACON 90, 18~25.

Tuah, H. and Hudspeth, R. T., 1982. Comparisons of numerical random sea simulations, *J. Waterway, Port, Coastal and Ocean Eng.*, ASCE, **108**, 569~584.